# Chlorine-Catalyzed Ozone Destruction: Cl Atom Production from ClOOCl Photolysis

**David M. Wilmouth,* Thomas F. Hanisco,*,† Richard M. Stimpfle, and James G. Anderson**

*Department of Chemistry and Chemical Biology, Harvard University, Cambridge, Massachusetts, 02138*

*Received: June 5, 2009; Revised Manuscript Received: September 10, 2009*

Recent laboratory measurements of the absorption cross sections of the ClO dimer, ClOOCl, have called into question the validity of the mechanism that describes the catalytic removal of ozone by chlorine. Here we describe direct measurements of the rate-determining step of that mechanism, the production of Cl atoms from the photolysis of ClOOCl, under laboratory conditions similar to those in the stratosphere. ClOOCl is formed in a cold-temperature flowing system, with production initiated by a microwave discharge of $Cl_2$ or photolysis of $CF_2Cl_2$. Excimer lasers operating at 248, 308, and 352 nm photodissociate ClOOCl, and the Cl atoms produced are detected with time-resolved atomic resonance fluorescence. $Cl_2$, the primary contaminant, is measured directly for the first time in a ClOOCl cross section experiment. We find the product of the quantum yield of the Cl atom production channel of ClOOCl photolysis and the ClOOCl absorption cross section, $(\phi\sigma)_{ClOOCl} = 660 \pm 100$ at 248 nm, $39.3 \pm 4.9$ at 308 nm, and $8.6 \pm 1.2$ at 352 nm (units of $10^{-20}$ $cm^2$ $molecule^{-1}$). The data set includes 468 total cross section measurements over a wide range of experimental conditions, significantly reducing the possibility of a systematic error impacting the results. These new measurements demonstrate that long-wavelength photons ($\lambda = 352$ nm) are absorbed by ClOOCl directly, producing Cl atoms with a probability commensurate with the observed rate of ozone destruction in the atmosphere.

## Introduction

On the global scale, with little doubt, the most successful intersection of fundamental science and public policy is the case linking ground-level chlorofluorocarbon (CFC) release with the chlorine-catalyzed loss of ozone in the Earth's stratosphere. This scientific case led to the Montreal Protocol, with its subsequent London and Copenhagen amendments, which controls the global release of CFCs. The scientific case was built on what was thought to be an unequivocal combination of laboratory experiments and in situ and remote observations of the stratosphere.[1]

ClOOCl is the centerpiece of the catalytic cycle (Figure 1a) that accounts for more than 50% of the chlorine-catalyzed ozone loss in the Arctic and Antarctic stratosphere every spring.[2] In this mechanism,[3] the photolysis of ClOOCl to produce Cl atoms is the rate-determining step for the removal of $O_3$ by chlorine:

$$2ClO + M \rightleftarrows ClOOCl + M \quad (1a)$$

$$ClOOCl + h\nu \rightarrow Cl + ClOO \quad (2a)$$

$$ClOO + M \rightarrow Cl + O_2 + M \quad (3)$$

$$2(Cl + O_3 \rightarrow ClO + O_2) \quad (4)$$

$$\text{Net: } 2O_3 \rightarrow 3O_2 \quad (5)$$

Critical in this cycle is the production of two Cl atoms from the photolysis of ClOOCl. If the photolysis reaction produced ClO, a null cycle would result, and $O_3$ would not be destroyed:

$$2ClO + M \rightleftarrows ClOOCl + M \quad (1a)$$

$$ClOOCl + h\nu \rightarrow 2ClO \quad (2b)$$

Net: null

The photolysis rates of ClOOCl in the atmosphere are directly related to the absorption cross sections. Recently, Pope et al.[4] reported dramatically smaller absorption cross sections for ClOOCl in the critical wavelength region between 300 and 400 nm. Taken alone, this result would indicate an unknown mechanism must be responsible for the dramatic ozone loss observed in the Arctic and Antarctic every spring. However, when considered along with the body of laboratory work both prior and since its publication, this study has instead served to

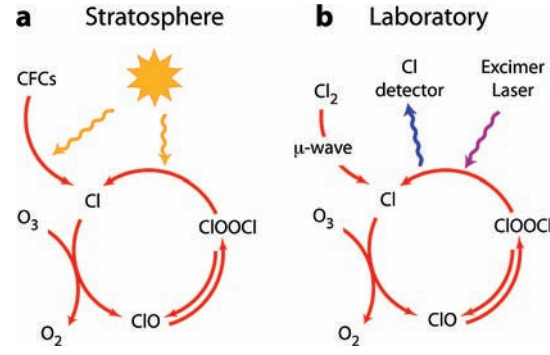


**Figure 1.** Catalytic removal of ozone by chlorine. (a) Chlorine released from CFCs removes ozone as it forms ClO. The subsequent formation of ClOOCl is the critical point in the cycle: thermal decomposition back to ClO short circuits the cycle, resulting in no net ozone loss, while photolysis with relatively abundant long-wavelength photons ($\lambda > 320$ nm) completes this cycle every few minutes. (b) The laboratory equivalent uses multiple excimer lasers to photolyze a continuous flow of ClOOCl at stratospheric conditions.

* To whom correspondence should be addressed. D.M.W.: e-mail, wilmouth@huarp.harvard.edu; phone, 617-495-5922; fax, 617-495-4902. T.F.H.: e-mail, thomas.hanisco@nasa.gov; phone, 301-614-6598.

† Currently at NASA Goddard Space Flight Center, Greenbelt, MD 20771.

10.1021/jp9053204 
Published on Web 10/23/2009

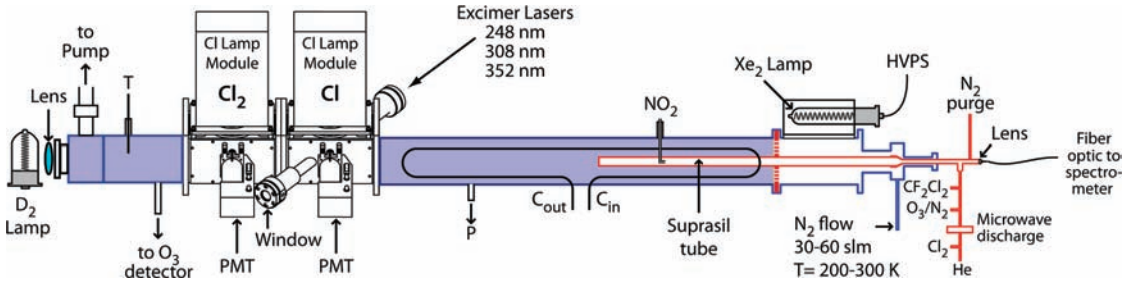


**Figure 2.** Schematic of the experimental apparatus. We photodissociate ClOOCl in a fast-flow system with excimer lasers operating at 248, 308, and 352 nm, detecting Cl atoms with atomic resonance fluorescence and $Cl_2$ with nonresonant molecular fluorescence.

highlight the inconsistency in measurements of the absorption cross section using traditional absorption spectroscopy techniques.[5]

Virtually all past laboratory measurements of the ultraviolet cross sections of ClOOCl utilized absorption spectroscopy. The primary challenge with this technique is that a number of other absorbing species, either added or produced when chemically forming ClOOCl, may be present in the absorption cell. In particular, the uncertainty in correcting ClOOCl spectra for the presence of $Cl_2$, which has an unstructured absorption signal that peaks at approximately 330 nm, has led to reported ClOOCl cross sections that differ by more than an order of magnitude in some of the most atmospherically relevant wavelength regions.[5]

Clearly, much of the confidence in the Molina mechanism[3] is based on the historically good agreement between model calculations and atmospheric observations of ozone loss, not on the solidity of the laboratory data set. The fundamental question remains: What is the photolytic efficiency to produce chlorine atoms from ClOOCl directly at atmospherically relevant conditions?

To address this question, we designed an experiment to couple the photolysis of ClOOCl at three excimer laser wavelengths (248, 308, and 352 nm) with direct, time-resolved detection of chlorine atoms. We measure the photodissociation cross section of ClOOCl for the photolysis pathway that produces Cl atoms, i.e., the product of the ClOOCl absorption cross section and the quantum yield of reaction 2a. This measured quantity is henceforth referred to simply as the photodissociation cross section, with the understanding that it is only a measure of photolysis channel 2a and does not include 2b. As defined and measured here, the photodissociation cross section is the quantity of greatest importance for the rate-limiting step of the ClOOCl catalytic cycle. Our experiments are conducted at conditions relevant to the atmosphere in a temperature-controlled fast-flow system that is designed to mimic the essential elements of the Molina mechanism (Figure 1b).

This approach has the scientific advantage that the production of Cl from ClOOCl photolysis is measured directly, thus providing an unambiguous laboratory measurement of the rate-limiting step in the ClOOCl mechanism. Moreover, this approach has the technical advantage of having detection sensitivity to Cl atoms in the parts per trillion range. Importantly, $Cl_2$ is measured for the first time in a study of the cross section of ClOOCl, here with a nonresonant molecular fluorescence technique developed for this experiment.

Since the completion of our laboratory work, measurements of the ClOOCl cross section at 308 and 351 nm have been reported by Chen et al.[6] using molecular beams with mass detection rather than absorption spectroscopy. This study reports the highest 351-nm ClOOCl cross section to date, a value that is approximately 60% higher at 250 K than the current JPL panel recommendation[7] (hereafter JPL-06) and a factor of 18 higher than that of Pope et al.[4] Clearly, resolving the discrepancy in reported values at this atmospherically relevant wavelength is of substantial importance in quantifying the role of ClOOCl in stratospheric ozone loss.

## Experimental Section

A diagram of the laboratory apparatus is shown in Figure 2. The main flow tube consists of a 7.6 cm × 7.6 cm square duct, approximately 2 m in length. Source gases and carrier gases are added to the right of the flow system as shown, with the direction of flow from right to left. The entire flow system resides inside a cooled, insulated box to aid in achieving low-temperature operation. Cooling originates in three locations: (1) the main $N_2$ carrier gas is cooled before entering the flow system by passing through a copper coil submerged in a dry ice/ethanol bath, (2) a Neslab chiller pumps cold ethanol through copper tubing attached to the metal flow tube walls, and (3) the air inside the insulated box is cooled with an attached liquid nitrogen tank. Pressure transducers are located at the center of the flow tube, and temperature readings are taken inside the flow system at the front and rear, along with a number of other thermistors deployed throughout the insulated box. The observed temperature gradient along the flow system is typically less than 4 K.

**ClOOCl Source Chemistry.** We employ two methods of source chemistry to generate ClOOCl. Our primary method is passing $Cl_2$/He through a microwave discharge to form Cl atoms (eq 6), followed by reaction with $O_3$ to form ClO (eq 4), which subsequently self-reacts at low temperatures to form ClOOCl (eq 1a).

$$Cl_2 \rightarrow 2Cl \qquad (6)$$

Our second method of ClOOCl formation uses $CF_2Cl_2$ photolysis[8] as the source of Cl atoms to react with $O_3$:

$$CF_2Cl_2 + h\nu_{172nm} \rightarrow CF_2Cl + Cl \qquad (7)$$

Photolysis of $CF_2Cl_2$ is accomplished using a high-intensity 172-nm xenon excimer lamp. There is good overlap between the emission of the $Xe_2$ lamp and the ultraviolet cross sections of $CF_2Cl_2$ in this wavelength region.[9] Neither $CF_2Cl_2$ nor the $CF_2Cl$ fragment and its reaction products (e.g., $CF_2ClO_2$ from reaction with $O_2$) affect the measurements, as Cl atom production was not observed from these molecules at our laser wavelengths.

In addition to the primary channel for the ClO self-reaction that forms ClOOCl (eq 1a), several competing bimolecular reactions can also occur:

$$2ClO \rightarrow Cl_2 + O_2 \quad (1b)$$

$$2ClO \rightarrow ClOO + Cl \quad (1c)$$

$$2ClO \rightarrow OClO + Cl \quad (1d)$$

The formation of ClOOCl is substantially faster than the bimolecular reactions at our typical cold-temperature conditions, e.g., approximately 60 times faster at 240 K. Moreover, of the bimolecular channels, only reaction 1d has the potential to affect the experiment. Reaction 1b forms $Cl_2$, which we measure, and reaction 1c is effectively a null reaction, as ClO is re-formed in the source tube via reactions 3 and 4.

We achieve a typical $ClO_x$ yield of 40−50% with the microwave discharge source and less than 1% using the photolysis lamp source. Photolyzing $CF_2Cl_2$ results in significantly smaller $Cl_2$ concentrations relative to ClOOCl than does passing $Cl_2$ through the microwave discharge.

The reactions of the photolysis source take place entirely inside a 75-cm long, 2.2-cm diameter UV-grade fused silica (Suprasil) tube embedded in the center of the main flow duct, as shown in Figure 2. The chemistry of the microwave discharge source also primarily occurs inside the Suprasil tube after being initiated in a fused silica side arm. Using a smaller diameter source region relative to the main duct enables higher ClO concentrations to be realized, which is essential for significant ClOOCl formation.[10,11]

At the end of the Suprasil tube, the source gases mix with a 30 standard-L $min^{-1}$ $N_2$ carrier gas in the larger 7.6-cm square duct, diluting all mixing ratios from the source by a factor of ~40 and essentially preventing any further source chemistry from taking place. Diluting the source flow in the main duct provides for low Cl concentrations in the detector region, which is necessary for accurate resonance fluorescence detection. Our "standard" experimental conditions include a duct pressure of 65 mbar, flow velocity in the duct of 110 cm $s^{-1}$, and temperature of 240 K. All experimental parameters were adjusted over a wide range of values during the course of the experiments.

$Cl_2$ is added from a 0.25% $Cl_2$/He cylinder, and $CF_2Cl_2$ is added from a 5% $CF_2Cl_2$/He cylinder. $O_3$ is formed by passing $O_2$ from a 10% $O_2$/Ar cylinder through an electric discharge to form approximately 5% $O_3/O_2$. Some experiments were performed in the absence of $O_2$ by trapping $O_3$ on silica gel.

**Photolysis and Detection.** Photolysis of ClOOCl in the flow system is accomplished using two copropogating excimer lasers operating with KrF (EX5, GAM Laser) and either XeCl or XeF fill gases (EX50, GAM Laser). The spectral output of the lasers was measured with a diode array spectrometer. The KrF laser output is centered at 248.43 nm and is approximated by a Gaussian function that is 0.5 nm wide (fwhm). The XeCl laser output is centered at 308.35 nm and is 0.9 nm fwhm. The XeF laser has two lines at 351 and 353 nm that are both 0.5 nm fwhm with an intensity ratio of 3:2. The average intensity-weighted wavelength of the XeF laser is ~351.8 nm. The laser wavelengths are rounded and stated as 248, 308, and 352 nm herein.

Figure 3 shows the absorption cross sections of ClOOCl from JPL-06 and Pope et al.[4] with the relevant excimer laser wavelengths indicated. The JPL-06 cross sections for ClO and $Cl_2$ are also shown for reference. As is evident in Figure 3, establishing the ClOOCl cross section at several select wavelengths is sufficient to resolve the large uncertainty surrounding the true value, especially at the atmospherically relevant longer wavelengths. Also evident in Figure 3, however, is that we do not photodissociate only ClOOCl at these wavelengths. Our measurement of $Cl_2$ and correction for ClO are addressed below. Here we simply note that the cross section of $Cl_2$ is insignificant at 248 nm, and the cross section of ClO is insignificant at 352 nm, simplifying any correction to the observed Cl signal.

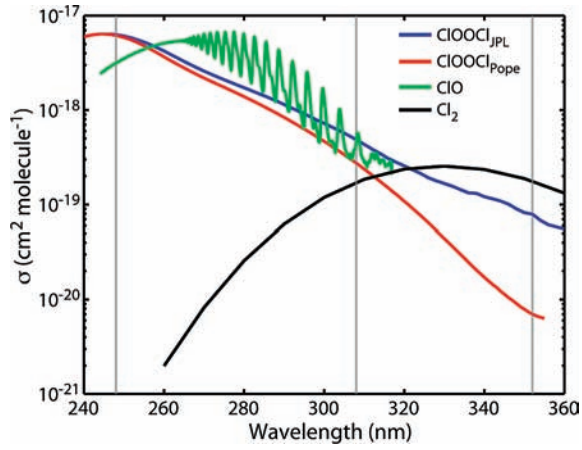


**Figure 3.** Absorption cross sections of ClOOCl from JPL-06 and Pope et al.,[4] along with JPL-06 cross sections of ClO and $Cl_2$ shown for reference. The excimer laser wavelengths are shown as vertical gray lines.

The laser light passes through the duct via the diagonal ports at the front and back sides of the first detection axis, as shown in Figure 2. Multiple apertures and knife-edged baffles are used to reduce scatter from the lasers. The optical setup ensures that the laser beams are well aligned and underfill the detection volume. Laser power is measured at the exit port of the flow duct. The lasers are typically operated at 75 Hz and 7.5 mJ $pulse^{-1}$.

There are two detection axes on the flow system, the first for measuring Cl atoms and the second for measuring $Cl_2$, as shown in Figure 2 and, in detail, in Figure 4. Cl detection at the first axis is accomplished using the well-established atomic resonance fluorescence technique.[12,13] The detection axis consists of a radio frequency-powered chlorine resonance lamp light source with a photomultiplier tube (KBr photocathode) detector at a right angle. Gas filter cells fitted with $MgF_2$ windows and pressurized with air are attached on both the lamp and PMT to isolate the 118.9-nm Cl lines. The photolysis lasers intersect the volume illuminated by the lamp and imaged by the PMT to maximize Cl fluorescence signal, as Cl is removed rapidly by the Cl + $O_3$ reaction.[14]

The Cl signal from the PMT is monitored with a multiscalar analyzer (Stanford Research Systems SR430). The signals are averaged into 50-$\mu$s bins and averaged for 3000 laser shots. The ability to resolve the fluorescence signal temporally is essential to isolating the prompt Cl atom signal from the photolysis of ClOOCl from any slower secondary processes affecting the Cl signal after photolysis.

The second Cl lamp axis is for $Cl_2$ detection via nonresonant molecular fluorescence.[15] The measurement of $Cl_2$ is required for correcting its contribution to the Cl atom signal at 308 and 352 nm, where the $Cl_2$ cross section is significant. The axis is operated with a $MgF_2$ window on the Cl lamp side, a sapphire

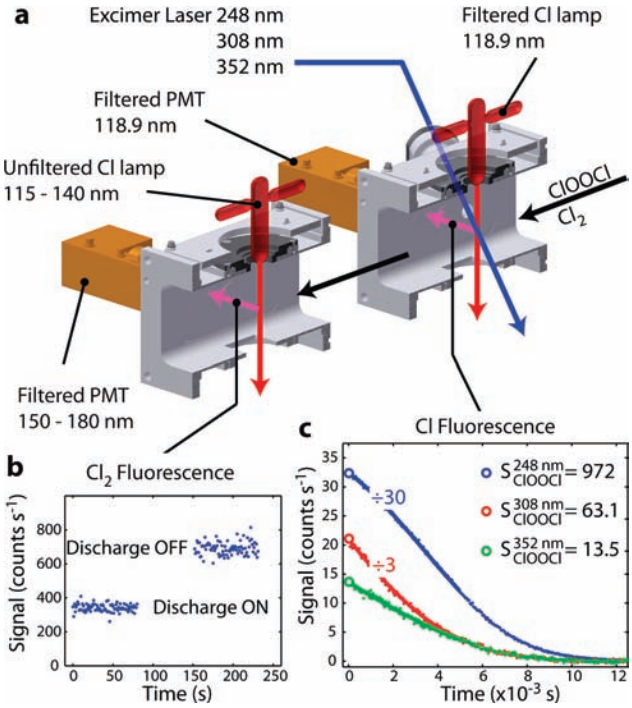


**Figure 4.** Detection geometry and signals. (a) Configuration of the excimer laser beams at the upstream Cl detection axis. The laser beams and Cl atom detection cross in the center of the flow tube. $Cl_2$ is measured downstream via molecular fluorescence using a similar detection axis. (b) Signal from the $Cl_2$ detector with the microwave discharge source on and off. The difference in $Cl_2$ signal is proportional to the amount of $Cl_2$ converted to ClOOCl. (c) Time-resolved Cl atom fluorescence resulting from photolysis of ClOOCl at 248, 308, and 352 nm. Signals are reported in 50-$\mu$s time bins and are normalized to the number of photons for 10 mJ pulse$^{-1}$ at 352 nm. The signal due to $Cl_2$ photolysis has been removed using the signal from panel b. The intercepts at time = 0 (open circles) are determined from polynomial fits to the data.

window on the PMT side, and $N_2$ in the filter cells. Multiple Cl emission lines between 130 and 140 nm are used to excite the $Cl_2$ $1^1\Sigma_u^+ - X^1\Sigma_g^+$ Rydberg series near 135 nm.[16] The red-shifted fluorescence of $Cl_2$ between 150 and 180 nm[17] is detected with near zero background by using the PMT filtered by a sapphire window that only transmits >150 nm. The sapphire window completely blocks all atomic Cl, O, and H fluorescence signals, allowing for a selective and unambiguous measurement of $Cl_2$.

We verified experimentally that the $Cl_2$ detector signal is unaffected by any other chemical species either added to the flow system or produced when the source is on. Moreover, because only very small fractions of ClOOCl and $Cl_2$ are photolyzed by the laser at 308 or 352 nm, the $Cl_2$ molecular fluorescence measurement is unaffected when the laser is on at these wavelengths. Both the Cl and $Cl_2$ detectors were calibrated with absorption at 118.9 nm across the duct and at 330 nm along the length of the source, respectively. While not used in the determination of the ClOOCl cross sections, these calibration runs are useful for scaling observed signals to concentrations, which can be compared with model results.

The ability to simultaneously detect Cl and $Cl_2$ with high sensitivity is an essential aspect of the experiment. An example of the relative sensitivity to $Cl_2$ of the molecular fluorescence axis and the Cl atomic fluorescence axis after photolysis at 352 nm is shown in Figure 5. For $[Cl_2] = 5.9 \times 10^{12}$ molecules cm$^{-3}$, the molecular fluorescence signal is 1200 counts s$^{-1}$, with a background signal of 30 counts s$^{-1}$. This gives a S/N = 1200/

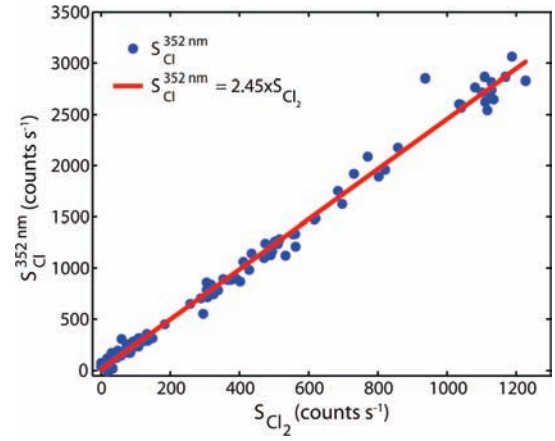


**Figure 5.** Signal from $Cl_2$ detected with Cl atom fluorescence after photolysis at 352 nm and with molecular fluorescence. The concentration of $Cl_2$ is varied between 0 and $5.9 \times 10^{12}$ molecules cm$^{-3}$. Conditions are $P = 65$ mbar and $T = 235$ K. The laser power is 8 mJ pulse$^{-1}$ at 75 Hz.

$1260^{1/2} = 34$ in 1-s integration, and S/N = 230 in the 45-s integration time used for these experiments. The detection limit for S/N = 1 in 45 s is $[Cl_2] = 5.8 \times 10^9$ molecules cm$^{-3}$. The Cl atomic detection is more sensitive, with S/N = 560 in 45-s integration; however, we use time-resolved detection with this method. For each 50-$\mu$s bin, the S/N = 23 for 45-s integration at a laser repetition of 75 Hz. Thus, for both Cl and $Cl_2$, the experiment yields excellent signal-to-noise ratios, which is important for identifying potential systematic errors.

Just downstream of the $Cl_2$ detection axis, a small fraction of the flow in the duct is continuously extracted (Figure 2) and passed through a multipass absorption cell to measure the $O_3$ concentration. An absorption path length of 600 cm is obtained with 20 passes of a 30-cm White cell. A mercury lamp at 254 nm is used as the light source, and a UV vacuum diode serves as the detector.

Concentrations of ClO, ClOOCl, OClO, $Cl_2$, and $O_3$ are measured periodically using UV absorption spectroscopy along the length of the source tube between 200 and 400 nm. The spectrometer is an Ocean Optics USB4000 with 0.7-nm bandwidth, fiber-coupled to the front end of the flow system, as shown in Figure 2. The light source is a Hamamatsu L6302 deuterium lamp located at the end of the duct.

**Calculating ClOOCl Cross Sections.** A key strategy in this study is that photodissociation cross sections of ClOOCl are determined by two independent methods. In method 1, the observed signal from ClOOCl at 308 or 352 nm is referenced to the observed signal and known cross section of ClOOCl at 248 nm:

$$(\phi\sigma)^{\lambda}_{\mathrm{ClOOCl}} = (\phi\sigma)^{\lambda_{\mathrm{ref}}}_{\mathrm{ClOOCl}} \frac{S^{\lambda}_{\mathrm{ClOOCl}}}{S^{\lambda_{\mathrm{ref}}}_{\mathrm{ClOOCl}}} \qquad (8)$$

where $\lambda$ is 308 or 352 nm and $\lambda_{\mathrm{ref}}$ is 248 nm; $(\phi\sigma)_{\mathrm{ClOOCl}}$ is the ClOOCl photodissociation cross section, i.e., the product of the quantum yield of the Cl production pathway (eq 2a) and the absorption cross section of ClOOCl at the indicated wavelength; and $S_{\mathrm{ClOOCl}}$ is the observed Cl atom signal from ClOOCl photolysis, normalized for the number of laser photons at that wavelength.

Method 2 is only valid for the microwave discharge source. Here the photodissociation cross section is determined by

referencing the observed signal from ClOOCl to the observed loss of $Cl_2$ when the discharge is turned on and to the known cross section of $Cl_2$ at 308 or 352 nm. This method relies on the conservation of chlorine between $Cl_2$ and ClOOCl; i.e., the concentration of ClOOCl is equal to that of $Cl_2$ that is removed. Model results, absorption spectroscopy, and laboratory diagnostic tests confirm that indeed nearly all (typically >95%) of the total Cl produced from $Cl_2$ is found in ClOOCl, as discussed below. The signal from the photolysis of ClOOCl is referenced to the $Cl_2$ cross section and the signal from the amount of $Cl_2$ that is removed:

$$(\phi\sigma)^{\lambda}_{ClOOCl} = (\phi\sigma)^{\lambda_{ref}}_{Cl_2}\frac{S^{\lambda}_{ClOOCl}}{\Delta S^{\lambda_{ref}}_{Cl_2}} \quad (9)$$

where $\lambda = \lambda_{ref}$ when $\lambda$ is 308 or 352 nm, and $\lambda_{ref}$ is 308 or 352 nm when $\lambda$ is 248 nm; $(\phi\sigma)^{\lambda_{ref}}_{Cl_2}$ is the photodissociation cross section of $Cl_2$ at the reference wavelength; $\Delta S^{\lambda_{ref}}_{Cl_2}$ is the decrease in $Cl_2$ signal (observed at the $Cl_2$ detection axis and normalized to the Cl detection axis using a scaling factor appropriate for the reference wavelength) when the microwave discharge is turned on; and other variables are as defined for eq 8.

Because both methods of determining the photodissociation cross section simply involve a ratio of two signals multiplied by a reference cross section, there is no need to know absolute concentrations of the molecules in the flow tube. Using the reference cross sections of ClOOCl at 248 nm and $Cl_2$ at 308 and 352 nm, the cross section of ClOOCl can be determined a variety of ways for our three laser wavelengths using both calculation methods and the two source chemistry techniques.

**Experimental Procedure.** Each ClOOCl cross section measurement is determined from a set of four consecutive laboratory runs: (1) 248-nm laser photolysis with the ClOOCl source on; (2) 308- or 352-nm laser photolysis with the ClOOCl source on; (3) 308- or 352-nm laser photolysis of $Cl_2$ only with the ClOOCl source off; and (4) background measurement with the source, lasers, and $Cl_2$ off. Runs 1−3 each consist of an average of 3000 laser shots. Ozone is maintained at a constant concentration for each set of runs.

The ratio of signals at the two detectors with only $Cl_2$ added to the flow in run 3 is used to determine the scaling factor that relates the relative sensitivity of the detection axes to $Cl_2$. The measured $Cl_2$ signal at the molecular fluorescence detector in run 2 is multiplied by this scaling factor to determine the amount of signal due to $Cl_2$ photolysis at the Cl atomic fluorescence detector. This $Cl_2$ contribution is subtracted from the total Cl signal in run 2 to yield the Cl signal from ClOOCl alone at 308 or 352 nm.

Sample signals observed from the $Cl_2$ detector and the Cl detector using the three photolysis wavelengths are shown in Figure 4b,c. The signal from the $Cl_2$ detector, depicted in Figure 4b, is used to correct the signal at the Cl detector for $Cl_2$ that is photolyzed at 308 or 352 nm. For method 2, the difference in signals with the microwave discharge off and on is used to calculate the amount of $Cl_2$ converted to ClOOCl in the source. Figure 4c shows time-resolved Cl atom fluorescence signals from the photolysis of ClOOCl. The signal decay as a function of time for each trace is due to the reaction of Cl with $O_3$, as well as Cl moving out of the detection volume. In this example, the signal resulting from the photolysis of $Cl_2$ has been removed. This $Cl_2$ signal is approximately twice that of ClOOCl at 352 nm and half that of ClOOCl at 308 nm.

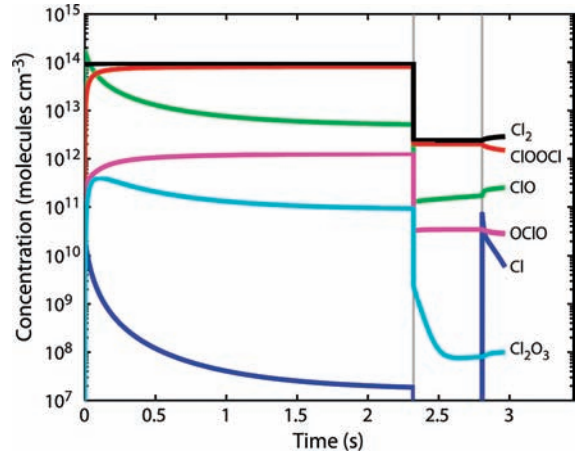


**Figure 6.** Photochemical model output for $P = 65$ mbar and $T = 240$ K with initial $Cl_2 = 1.8 \times 10^{14}$ molecules cm$^{-3}$ and initial $O_3 = 6.5 \times 10^{14}$ molecules cm$^{-3}$. The vertical gray lines mark (1) the dilution from the Suprasil source tube into the main flow duct and (2) the location of the laser photolysis axis.

The value of interest in each trace in Figure 4c is the *y*-intercept, i.e., the prompt Cl atom signal from ClOOCl photolysis that is unaffected by secondary chemistry. The *y*-intercept is determined for each trace from a polynomial fit to the data. The polynomial fits have a precision of ±10−20%. With these *y*-intercept values representing $S_{ClOOCl}$, and $\Delta S^{\lambda_{ref}}_{Cl_2}$ easily determined from the $Cl_2$ detector data and the $Cl_2$ scaling factor run (not shown), the ClOOCl photodissociation cross sections in eqs 8 and 9 are calculated.

Our Cl detection is only sensitive to ground-state Cl atoms ($^2P_{3/2}$). During the course of these experiments, we determined that approximately 10% of the Cl atoms produced from the photolysis of ClOOCl at 248 nm were in the excited state ($^2P_{1/2}$). The time required for quenching the excited state with $N_2$ in these experiments was ∼500 $\mu$s, which is easily detected and could lead to an undercounting of the Cl signal from the 248-nm laser photolysis. Collisions with $CF_2Cl_2$ rapidly deactivate Cl ($^2P_{1/2}$).[18] We found that adding a small amount of $CF_2Cl_2$ ($2 \times 10^{14}$ molecules cm$^{-3}$) reduced the quenching time below our sampling time resolution.

## Results and Discussion

**Kinetic Model and Spectroscopy of the Source.** Because the reactions initialized by the microwave discharge or $Xe_2$ photolysis lamp set off a complex photochemical mechanism, a kinetic model of the flow tube is used to aid in understanding and optimizing the flow chemistry. A reaction set including all known relevant photochemical reactions is used in the model. The kinetic rate constants and equilibrium constants are taken from JPL-06 with the exception of the ClOOCl equilibrium constant, which is from Plenge et al.[19] The Plenge et al. value is smaller than that of JPL-06 by a factor of approximately 2.6 at 240 K and is in better agreement with high-altitude aircraft measurements.[20−22] The model is run for a broad range of possible temperatures, pressures, and concentrations. Typical model output for a microwave discharge run at 240 K with the 248-nm laser is presented in Figure 6, where the evolution of the chlorine species is shown as a function of time.

The modeled concentrations of $Cl_2$, ClOOCl, and $O_3$ (not shown) agree well with those that we observe in the laboratory in the source and detector regions. $Cl_2$ and ClOOCl are roughly equal for the discharge source. Model runs and laboratory experiments both show that the $CF_2Cl_2$ photolysis source has

**TABLE 1: Concentrations of Molecules at the Laser Photolysis Axis from the Photochemical Model Run in Figure 6**

| | | $fClO_x$[a] | |
|---|---|---|---|
| molecule | concentration (molecules $cm^{-3}$) | Plenge et al. | JPL-06 |
| $Cl_2$ | $2.39 \times 10^{12}$ | | |
| ClOOCl | $2.00 \times 10^{12}$ | 95.1 | 96.6 |
| ClO | $1.70 \times 10^{11}$ | 4.04 | 2.65 |
| OClO | $3.40 \times 10^{10}$ | 0.81 | 0.79 |
| $Cl_2O_3$ | $8.03 \times 10^{7}$ | 0.0038 | 0.0025 |

[a] The fraction (in percent) of Cl released from $Cl_2$ found in each $ClO_x$ species for model runs using the Plenge et al.[19] and JPL-06 equilibrium constants.

less $Cl_2$ present, but we find that it is not possible to be free of $Cl_2$ due to the very fast[7] reaction of Cl atoms with ClOOCl,

$$Cl + ClOOCl \rightarrow Cl_2 + ClOO \qquad (10)$$

For both sources, the concentrations of all other chlorine oxides are substantially less than that of ClOOCl. Table 1 lists the concentrations of the chlorine species at the laser photolysis axis for the model run shown in Figure 6. The fraction of $ClO_x$ ($= 2ClOOCl + ClO + OClO + 2Cl_2O_3$) represented by each molecule is also shown.

The model indicates that 95−97% of the Cl atoms produced from $Cl_2$ are found in ClOOCl at the laser photolysis axis for these typical experimental conditions. The remainder is found in ClO (2−4%) and OClO (<1%). The concentration of $Cl_2O_3$ is negligible. A series of model runs testing all temperatures, pressures, velocities, and concentrations used in this experiment, along with varying the ClOOCl equilibrium constant, indicate that ClOOCl typically comprises at least 95% of $ClO_x$ and always comprises at least 90% of $ClO_x$, as long as the temperature is less than 250 K.

Absorption spectra of the source species were obtained in the laboratory using the 110-cm combined length of the Suprasil tube and fused silica side arm as the absorption path. The diluted flow in the main duct (Figure 2) does not significantly affect the absorption. A typical spectrum is shown in Figure 7 along with least-squares fits using JPL-06 cross sections. Background and sample spectra were obtained with the microwave discharge source off and on, respectively. Ozone concentrations were held nearly constant; a small ozone residual was removed with the fitting and is not shown. The concentrations determined from the least-squares fits represent the mean values within the source tube, i.e., the first 2.3 s of Figure 6. The concentration of ClOOCl at the end of the source region is higher than the mean value, and that of ClO is lower, as ClO forms the dimer as it progresses down the tube. Spectra obtained with different velocities and temperatures in the source show different relative abundances of OClO and ClO, as expected.

Overall, the spectroscopic results are consistent with the kinetic model and confirm that the chemistry in the flow system is understood. The only $ClO_x$ species observed in the spectra are ClOOCl, ClO, and OClO. The concentrations determined from the least-squares fits in Figure 7 correspond to a percent contribution to $ClO_x$ of 86.0 for ClOOCl, 13.7 for ClO, and 0.26 for OClO. These values are in excellent qualitative agreement with the model results in Table 1. The quantitative differences in ClO and ClOOCl are expected, as the start of source region averaged into the spectra has high ClO and low ClOOCl concentrations.

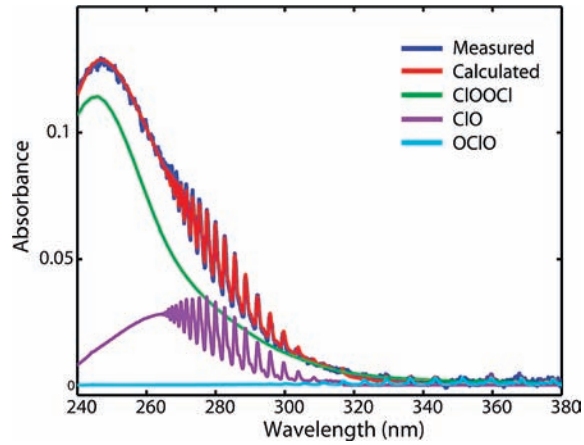


**Figure 7.** Absorption spectrum of the ClOOCl source. The spectrum is acquired along the 110-cm length of the source tube at $P = 65$ mbar and $T = 245$ K with the $Cl_2$/He microwave discharge source. A least-squares fit to the spectrum with the contributing ClOOCl, ClO, and OClO components are shown. The average concentrations ($\times 10^{14}$ molecules $cm^{-3}$) obtained from the least-squares fit to the spectrum are [ClOOCl] = 1.66, [ClO] = 0.53, and [OClO] = 0.01.

**TABLE 2: Absorption Cross Sections of Molecules in the Flow System at the Excimer Laser Wavelengths[a]**

| molecule | $\sigma^{248nm}$ | $\sigma^{308nm}$ | $\sigma^{352nm}$ |
|---|---|---|---|
| ClOOCl | 632 | 48.6 | 7.9 |
| $Cl_2$ | <0.1 | 17.3 | 17.8 |
| ClO | 315 | 47.7 | <1 |
| $ClONO_2$ | 62.4 | 1.8 | 0.22 |
| $O_3$ | 1080 | 12.2 | 0.03 |

[a] Cross sections are from JPL-06 and have units of $10^{-20}$ $cm^2$ $molecule^{-1}$. $ClONO_2$ is only relevant for the experiments where $NO_2$ is added.

**Consideration of Potential Interferences.** ***Chemical.*** The kinetic model and laboratory absorption spectra both show that ClOOCl and $Cl_2$ are the dominant chlorine-containing molecules in the flow system, with ClO and OClO present in minor concentrations. There is no evidence for a significant presence of any other $ClO_x$ species. These results, along with other exploratory laboratory diagnostic tests over a wide range of experimental conditions, give confidence that all significant chlorine-containing molecules in the flow system have been identified. This is of critical importance, as the generation of chlorine atoms from laser photolysis of a molecule that is not accounted for will bias the chlorine atom yield measurements.

Absorption cross sections of several important molecules in the flow system are shown in Table 2 at the relevant excimer laser wavelengths. OClO is not shown in Table 2, as tests at room temperature, where the concentration is much higher, show no measurable Cl atom production when OClO is photolyzed. Because $Cl_2$ is measured, the only significant chlorine species in the flow system not explicitly accounted for is ClO.

The significance of ClO laser photolysis at 248 and 308 nm is calculated using results from the kinetic model. The fractional contribution of Cl atoms from photolysis of ClO relative to that from ClOOCl is the ratio of the concentrations and cross sections, assuming unity quantum yield, with a factor of 2 accounting for the two Cl atoms per ClOOCl molecule:

$$Cl_{ClO}/Cl_{ClOOCl} = 1/2[ClO]/[ClOOCl] \times \sigma_{ClO}/\sigma_{ClOOCl} \qquad (11)$$

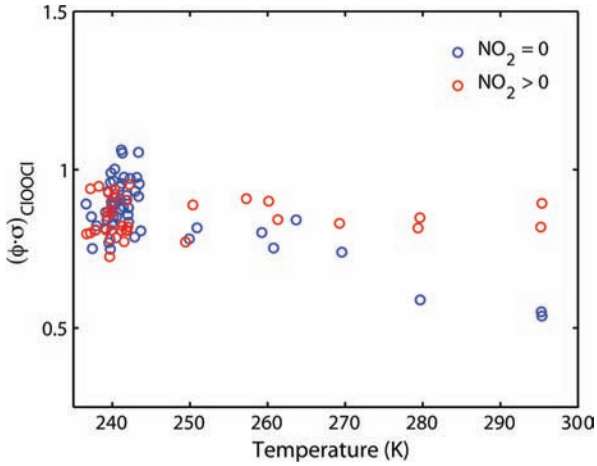


**Figure 8.** Photodissociation cross sections of ClOOCl at 352 nm (units of $10^{-20}$ cm$^2$ molecule$^{-1}$) with and without $NO_2$ added to the flow versus temperature. The cross sections are determined from the ratio of signals obtained at 352 and 248 nm (method 1). The difference in the measured values with and without $NO_2$ results from the presence of ClO. This difference only becomes significant at $T > 250$ K.

The model indicates that [ClO]/[ClOOCl] = 0.08 ± 0.04 over the range of our typical experimental conditions, depending on which ClOOCl equilibrium constant is used. At 248 nm, we expect the contribution of ClO photolysis to be 0.5 × 0.08(±0.04) × 315/632 = 0.02 ± 0.01 relative to that of ClOOCl photolysis. At 308 nm, we expect a larger contribution of 0.04 ± 0.02. Accordingly, we include a 2% correction for ClO photolysis at 248 nm and a 4% correction for ClO photolysis at 308 nm in our reported ClOOCl cross sections. The inclusion of these corrections is also factored into the reported uncertainties. We verified that ClO does not produce measurable Cl atoms at 352 nm in experiments performed at room temperature.

The small impact of ClO photolysis predicted by the model was confirmed in the laboratory by adding $NO_2$ to the source flow to remove ClO via

$$ClO + NO_2 + M \rightarrow ClONO_2 + M \qquad (12)$$

Since the cross section of $ClONO_2$ is approximately a factor of 10 smaller (Table 2) than that of ClOOCl, and the Cl photolysis yield is less than unity,[7] $NO_2$ effectively removes ClO from the system by converting it to $ClONO_2$. We therefore expect that the cross section measured at 352 nm using 248 nm as a reference should be 2% higher and that the cross section at 308 nm should be 2% lower with $NO_2$ present (eq 8). Measurements with and without $NO_2$ are nearly identical for most of the conditions of the experiments, indicating that ClO concentrations in the flow tube are indeed small. The exception is for $T > 250$ K when the ClO/ClOOCl ratio is larger. Figure 8 shows photodissociation cross sections determined at 352 nm to illustrate this result.

In addition to the ClO photolysis correction, a second minor correction to the method 2 results is necessary to account for the fact that $Cl_2$ lost in the microwave discharge equals approximately 95% (Table 1) of the ClOOCl formed instead of 100%. Accordingly, our reported 352-nm ClOOCl cross section results with method 2 are increased by 5% from those measured to account for the 5 ± 2% of $ClO_x$ in ClO or OClO at the typical experimental conditions where the measurements were made (eq 9). The correction to the measured values is only 1% for the ClOOCl cross section at 308 nm referenced to $Cl_2$ and 3% at 248 nm, due to the compensating 4% Cl signal from ClO photolysis at 308 nm and the 2% Cl signal from ClO photolysis at 248 nm.

It is important to emphasize that no large correction to our measured ClOOCl photodissociation cross sections is necessary due to unmeasured interfering species. The aforementioned minor corrections could in fact be ignored without significantly changing our cross section results. No value is adjusted by more than 5% from what was measured, and the corrections applied to most reported values are less than 2%.

One final consideration with regards to chemical interferences is the potential for secondary chemistry reactions to affect the observed Cl signal. Two important reactions initiated after laser photolysis are Cl + $O_3$ that removes Cl atoms (eq 4) and

$$O + ClO \rightarrow Cl + O_2 \qquad (13)$$

that produces Cl atoms. The latter reaction is only important at 248 nm, where the $O_3$ cross section is substantially greater than at 308 or 352 nm (Table 2). The photolysis of $O_3$ with the 248-nm laser produces O atoms, which react rapidly with ClO produced from the Cl + $O_3$ reaction.

The impact of the O + ClO reaction producing Cl atom signal after ClOOCl photolysis can be substantial. Chlorine atoms that are regenerated via cycling through eqs 4 and 13 can contribute to the fluorescence signal multiple times before passing through the detection volume. This is the primary reason why having time-resolved fluorescence detection for this experiment is essential. Our laboratory results and kinetic model both show clearly that the use of the prompt Cl signal (*y*-intercept) in our time-resolved fluorescence detection eliminates any influence from secondary chemistry reactions on our results. In general, no secondary chemistry reactions are fast enough to affect the prompt Cl signal observed from ClOOCl photolysis. We also note that the ClOO fragment from ClOOCl photolysis dissociates so rapidly that we observe both Cl atoms from ClOOCl promptly, even with time-resolved detection.

***Wall Loss.*** If present, loss of ClOOCl on surfaces of the flow system could significantly impact the measurements. Specifically, if ClOOCl were lost on the walls, the photodissociation cross sections determined using method 2 may be biased low, as the observed loss of $Cl_2$ would overestimate the amount of ClOOCl actually present (eq 9). In general, the method 1 results should be unaffected by wall loss.

Previous laboratory studies note the potential for ClOOCl to be lost on surfaces and employ the use of clean quartz tubing or a halocarbon wax coating on the walls to minimize its destruction.[4,23−25] Similarly, our source tube, where ClOOCl typically resides for 75% of its time in the flow system, is clean Suprasil. The main duct is electropolished stainless steel with an amorphous silicon coating from Restek.

To test for the possibility of surface loss affecting the measurements, we varied velocity in both the main flow duct and Suprasil source tube by factors of approximately 2 and 4, respectively. Panels a and b in Figure 9 show the photodissociation cross sections of ClOOCl at 352 nm for these velocity runs. If wall loss were significant, the measured photodissociation cross sections for method 2 would decrease at the lower velocities and increase at the higher velocities. The absence of any trend in the method 2 values indicates that the observed photodissociation cross sections are independent of exposure time to the walls and, therefore, are very unlikely to be biased by wall loss of ClOOCl (or any other chlorine species formed when the microwave discharge is turned on).

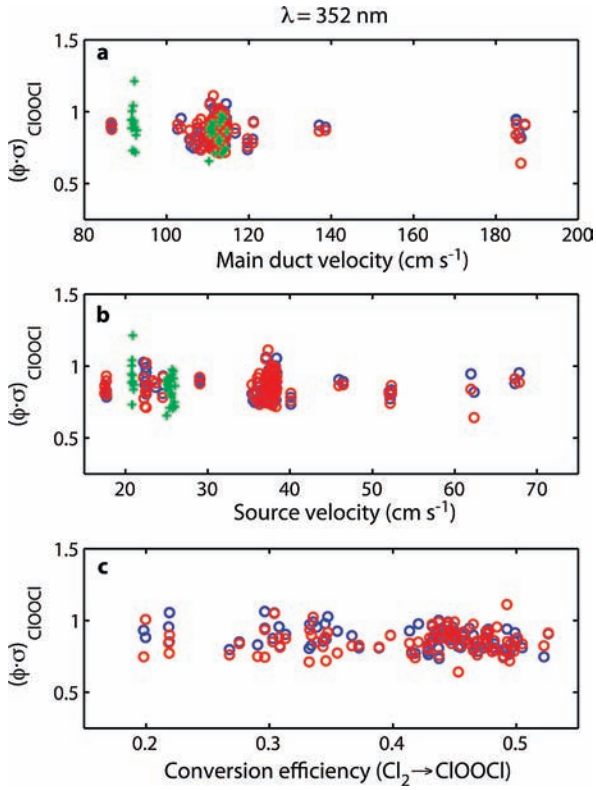


**Figure 9.** Photodissociation cross sections of ClOOCl at 352 nm (units of $10^{-20}$ cm$^2$ molecule$^{-1}$) versus (a) velocity in the main duct, (b) velocity in the Suprasil source tube, and (c) conversion efficiency of the microwave discharge, as determined from the $Cl_2$ molecular fluorescence detector. Data obtained with the photolysis source (+) are in green, and data obtained with the microwave discharge source (○) using method 1 are in blue and using method 2 are in red.

Further evidence that wall loss is not significant is shown in Figure 9c. The measured photodissociation cross sections of ClOOCl at 352 nm are independent of the conversion efficiency of the microwave discharge source, as measured at the $Cl_2$ detection axis. The absence of a systematic trend demonstrates that the photodissociation cross sections are not affected by the relative concentrations of chlorine species in the flow system and that wall loss is not biasing the observed conversion efficiency numbers.

The experimental evidence demonstrating that surface loss is not significant is consistent with results from past studies. Burkholder et al.[26] concluded that there was no wall loss of ClOOCl in their experiment after changing the residence time in their absorption cell by a factor of 3 and observing no systematic decrease in the ClOOCl absorption cross sections. Two studies using static cells quantified the decomposition of ClOOCl: Demore and Tschuikow-Roux[24] found a rate constant of approximately $1 \times 10^{-4}$ s$^{-1}$ at 195 K, and Cox and Hayman[23] reported a ClOOCl half-life of 1000 s at 233 K. These numbers imply a slow ClOOCl decay on surfaces with far less than 1% of ClOOCl lost in 3 s, the approximate residence time in our flowing system. We note that the temperatures used in our experiment are much too warm to condense ClOOCl on the walls, as in the Pope et al.[4] study.

In summary, if wall loss of ClOOCl is biasing our measurements, we are unable to identify or quantify it, so we do not employ any correction for wall effects to the data. We also note that even if ClOOCl were lost on the walls of our flow system, our measurements would essentially be unaffected if the loss mechanism produced $Cl_2$ as the product. Because our $Cl_2$ measurement is made near the end of the flow system, interchange between ClOOCl and $Cl_2$ upstream of the Cl atomic fluorescence axis has no impact on the method 2 cross sections.

**Photodissociation Cross Sections.** Figure 10 shows our ClOOCl photodissociation cross section results at 308 nm (upper grouping of points in each panel) and 352 nm (lower points). We performed 240 experiments over a wide range of conditions in search of any parameter that would influence our measured values. Figure 10 shows $(\phi\sigma)_{ClOOCl}$ determined from eqs 8 and 9 for every one of the 240 individual measurement runs acquired over several months. It is immediately clear from panel a that the data are tightly grouped with no apparent differences whether the cross section is measured with the microwave discharge source or $Xe_2$ photolysis lamp source or whether the calculation is made using method 1 or method 2. There is also no obvious temporal trend.

Panels b−e show the photodissociation cross sections plotted versus a number of variables that could potentially influence the results. The absence of any trend in these regressions confirms that a number of potential issues have been properly addressed. The absence of a slope in panel b indicates that $Cl_2$ is being measured and accounted for correctly. Panel c shows that there are no abnormalities in our detection of ClOOCl over a wide range of concentrations, panel d indicates that the measured signal is not influenced by any reaction that involves $O_3$, and panel e shows no cross section dependence on the pressure of the flow system. The trend with temperature at 352 nm in panel f is significant. When ClO is not fully converted to ClOOCl at $T > 250$ K, method 2 is not accurate, i.e., the $\Delta S^{\lambda ref}_{Cl_2}$ term in eq 9 is erroneously large. The scatter in Figure 10 results from statistical uncertainty of each measurement (±20−30%).

In addition to the regressions shown in Figures 8−10, the data set includes variations in $NO_2$ concentration, laser power, laser beam size and position, experimental order of data acquisition, and chlorine lamp output. We are unable to identify any experimental parameter at $T < 250$ K that can significantly change our results, giving confidence that the chemical flow system is well understood and that systematic errors have been identified and properly addressed.

A summary of all the cold-temperature ClOOCl cross section data is shown in Table 3. Because each of the 240 experimental runs is typically used to determine the ClOOCl cross section in more than one way, there are 468 total photodissociation cross section measurements represented here. The results are itemized on the basis of source chemistry, calculation method, and wavelength. The method 1 results are those referenced to ClOOCl at 248 nm, and the method 2 results are those referenced to $Cl_2$ at 308 and 352 nm. The columns listing the ratios of the photodissociation cross sections of the reference molecules to those of ClOOCl represent our experimentally determined values, i.e., the ratios of measured signals from eqs 8 and 9. Uncertainties in the ratios include the standard deviation of the measurements and an estimate of systematic error. The corrections that account for the presence of ClO and OClO are included in the systematic error. We report two values at 248 nm, three at 308 nm, and three at 352 nm.

Using the listed JPL-06 values for the reference cross sections and assuming a quantum yield of 1, the ClOOCl photodissociation cross sections for each of the eight ratio measurements are determined. The photodissociation cross section results agree remarkably well for each wavelength, independent of the source chemistry or calculation method. We note that our photodissociation cross section values should be revised in the future if the reference cross sections are changed.

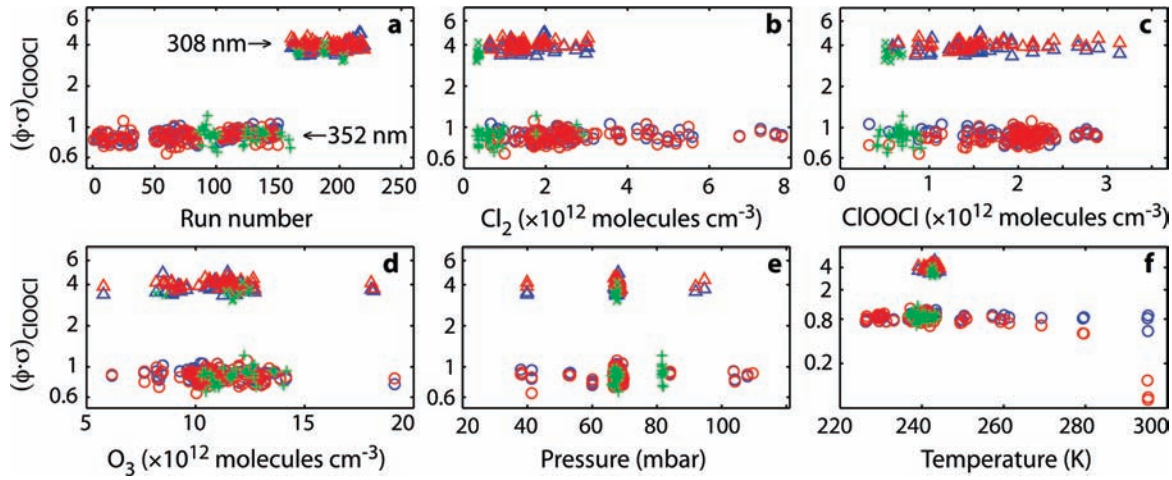


**Figure 10.** Photodissociation cross sections of ClOOCl (units of $10^{-20}$ cm$^2$ molecule$^{-1}$) for the photolysis pathway that produces Cl atoms. Data obtained with the photolysis source at 308 nm (×) and 352 nm (+) are in green. Data obtained with the microwave discharge source at 308 nm (Δ) and 352 nm (○) using method 1 are in blue and using method 2 are in red. The measurements are shown on a log scale plotted against (a) run number, (b) $Cl_2$ concentration, (c) ClOOCl concentration, (d) $O_3$ concentration, (e) pressure, and (f) temperature. Data in panels a−e are limited to $T < 250$ K. In panel f, $NO_2$ was added to remove excess ClO for $T > 250$ K.

**TABLE 3: Summary of Measured ClOOCl Photodissociation Cross Sections at T = 240 ± 10 K[a]**

| | | | 248 nm | | 308 nm | | 352 nm | |
|---|---|---|---|---|---|---|---|---|
| source | reference | $\sigma_{ref}$ | $(\phi\sigma)_{ref}/(\phi\sigma)_{ClOOCl}$ | $(\phi\sigma)_{ClOOCl}$ | $(\phi\sigma)_{ref}/(\phi\sigma)_{ClOOCl}$ | $(\phi\sigma)_{ClOOCl}$ | $(\phi\sigma)_{ref}/(\phi\sigma)_{ClOOCl}$ | $(\phi\sigma)_{ClOOCl}$ |
| microwave | $ClOOCl^{248nm}$ | 631.5 | — | — | 16.36 ± 1.82 | 38.6 | 72.67 ± 6.94 | 8.69 |
| photolysis | $ClOOCl^{248nm}$ | 631.5 | — | — | 17.59 ± 2.06 | 35.9 | 71.76 ± 9.54 | 8.80 |
| microwave | $Cl_2^{308nm}$ | 17.32 | 0.0257 ± 0.0029 | 675 | 0.431 ± 0.034 | 40.2 | — | — |
| microwave | $Cl_2^{352nm}$ | 17.78 | 0.0276 ± 0.0029 | 644 | — | — | 2.08 ± 0.23 | 8.54 |
| mean value | | | | 660 ± 100 | | 39.3 ± 4.9 | | 8.6 ± 1.2 |

[a] Photodissociation cross sections of ClOOCl are for the photolysis channel that produces Cl atoms (eq 2a). Cross sections are in units of $10^{-20}$ cm$^2$ molecule$^{-1}$. Reference cross sections are from JPL-06. Values for $(\phi\sigma)_{ClOOCl}$ are calculated assuming $\phi_{ref} = 1$. The mean photodissociation cross section for each wavelength, shown in the lowermost row, is the mean of all the individual measurements: 140 measurements at 248 nm, 92 at 308 nm, and 236 at 352 nm. Uncertainties in the mean values include the measurement and statistical uncertainties but not uncertainties from the reference cross sections.

The average photodissociation cross section for each wavelength is shown in the lowermost row of Table 3. The uncertainties listed are only the measurement and statistical uncertainties (∼12−15%) and do not include uncertainties for the reference cross sections from JPL-06.

**Perspective on Cross Section Results.** The value recommended by JPL-06 for the ClOOCl cross section at each laser wavelength is shown in Table 2. In comparing these numbers with those in Table 3 from this work, it is important to note that the JPL-06 values are absorption cross sections, while our values are the products of quantum yields and absorption cross sections. The quantum yield for the Cl atom production channel of ClOOCl photolysis (eq 2a) recommended by JPL-06 is 1.0(±0.1) below 300 nm and 0.9(±0.1) above 300 nm. If the quantum yield above 300 nm is indeed 0.9, our average 308- and 352-nm absorption cross sections are 43.7 and 9.6, respectively (units of $10^{-20}$ cm$^2$ molecule$^{-1}$).

To our knowledge, the quantum yield of reaction 2a has never actually been measured experimentally at 352 nm, nor at any wavelength above 308 nm. Moreover, there is not a clear consensus in the literature regarding the true value of the quantum yield at 308 nm, and it certainly may be unity.[14] The IUPAC subcommittee recommendation[27] is, in fact, for a quantum yield of 1.0 throughout the 200−398 nm range. Given the uncertainty, we have decided to proceed here with the simplest assumption that the quantum yield is 1.0 at all wavelengths, i.e., our comparisons below assume that $(\phi\sigma)_{ClOOCl}$ in this study represents the same quantity as the ClOOCl absorption cross section in previous measurements. We emphasize that the true value of the quantum yield at these wavelengths has no direct effect on our results; it only affects our ability to compare our results with JPL-06 and other previous studies that used absorption spectroscopy. The value we measure, the product of the quantum yield of the Cl production pathway and the ClOOCl absorption cross section, is the quantity of greatest atmospheric importance.

As is evident from Tables 2 and 3, the measurements of the photodissociation cross section in this study are similar to the values of the absorption cross section recommended by the JPL-06 panel at 248 and 352 nm but are slightly lower at 308 nm. That we agree with JPL-06 at 248 nm and are lower at 308 nm is not surprising, given the measurement database at those wavelengths.[5]

The cross section measurement at 352 nm is in many ways the most important result. The 352-nm wavelength is the most atmospherically relevant of those measured, and it is by far the most difficult to measure accurately with absorption spectroscopy, as the cross section of ClOOCl is small and that of $Cl_2$ is relatively large. Figure 11 shows the cross section of ClOOCl at 352 nm determined here and in many of the prior studies. The most striking feature of this figure is the wide range of values for the cross section and the corresponding large uncertainty estimate (factor of 3) in the JPL-06 recommendation.

Of the five previous individual cross section studies at 352 nm shown in Figure 11, Burkholder et al.[26] is the only study with which we have overlapping uncertainties. Our value is a

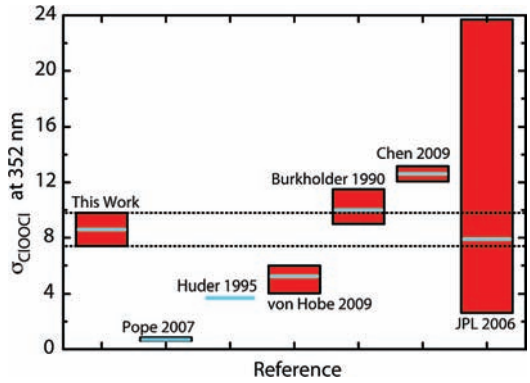


**Figure 11.** Absorption cross sections of ClOOCl at 352 nm (units of $10^{-20}$ cm$^2$ molecule$^{-1}$) from this work compared with selected previously published values.[4−7,25,26] The mean value for each study is shown in blue with stated error limits in red. The mean cross section from this work is shown assuming the quantum yield is 1.0 (see the text). The Pope et al.[4] uncertainty, which is obscured on the scale of this figure, is +20/−10%. Huder and DeMore[25] did not report uncertainties.

factor of 2.3 higher than that of Huder and DeMore,[25] which is also the IUPAC recommendation,[27] and a factor of 12 higher than that of Pope et al.[4] The recent Chen et al.[6] value at 250 K and 351 nm is 46% higher than our result. The source of the discrepancy is not clear, as their mass detection is not susceptible to the same impurity issues as the absorption studies, but we do not observe cross sections as high as those found in the five experimental runs of Chen et al.[6] at these conditions. Ultimately, we find our best cross section agreement at 352 nm with the JPL-06 recommended value. Our reported value is slightly higher than JPL-06, but our uncertainty range encompasses the recommendation.

It is worth considering the impact on these comparisons if the quantum yield of reaction 2a at 352 nm is actually 0.9 instead of 1.0. Overall, our cross section difference with most of the other studies is so substantial that any uncertainty regarding the quantum yield affecting the comparisons is inconsequential. One change of note is that our absorption cross section would be much closer to that of Burkholder et al.[26] than that of JPL-06, but our value would still lie between the two. While higher, the upper bound of our cross section uncertainty would remain significantly below the lower bound of the uncertainty from the Chen et al.[6] study.

Our relative agreement at 352 nm with the JPL-06 and Burkholder et al.[26] ClOOCl cross sections is consistent with ClO/ClOOCl field observations[1,20,28] and with the calculated ClOOCl photolysis rate that is needed to explain observed $O_3$ loss.[29] We find no need for new photolytic or reactive pathways to bring agreement between models and measurements of chemical ozone depletion.

## Conclusions

The photodissociation cross sections measured here are consistent with the widely accepted mechanism for chlorine removal by the ClOOCl catalytic cycle. The measurements show that the photolysis rate of ClOOCl is at least as fast as previously thought. Significantly, the likelihood of a large systematic error is greatly reduced by the measurement of the primary contaminant, $Cl_2$, and by a methodical variation in experimental conditions. The photolysis rates determined with these new data will not be substantially different from those determined with the values of JPL-06 or Burkholder et al.,[26] but the directness of the technique and completeness of this study help solidify the laboratory foundation supporting our understanding of chlorine-catalyzed ozone loss.

**Acknowledgment.** We appreciate the role of the SPARC initiative and workshop (The Role of Halogen Chemistry in Polar Stratospheric Ozone Depletion) in drawing focus to this scientific issue and promoting discussion. In particular, we thank Stan Sander, Jim Burkholder, and Kyle Bayes for helpful discussions on this work. This research is supported by NASA grant NNX09AE29G.

## References and Notes

(1) *World Meteorological Organization (WMO), Scientific Assessment of Ozone Depletion: 2006*, WMO Global Ozone Research and Monitoring Project, Report 50, WMO: Geneva, Switzerland, 2007.
(2) Frieler, K.; Rex, M.; Salawitch, R. J.; Canty, T.; Streibel, M.; Stimpfle, R. M.; Pfeilsticker, K.; Dorf, M.; Weisenstein, D. K.; Godin-Beekmann, S. *Geophys. Res. Lett.* **2006**, *33*, doi: 10.1029/2005GL025466.
(3) Molina, L. T.; Molina, M. J. *J. Phys. Chem.* **1987**, *91*, 433.
(4) Pope, F. D.; Hansen, J. C.; Bayes, K. D.; Friedl, R. R.; Sander, S. P. *J. Phys. Chem. A* **2007**, *111*, 4322.
(5) von Hobe, M.; Stroh, F.; Beckers, H.; Benter, T.; Willner, H. *Phys. Chem. Chem. Phys.* **2009**, *11*, 1571.
(6) Chen, H.; Lien, C.; Lin, W.; Lee, Y. T.; Lin, J. J. *Science* **2009**, *324*, 781.
(7) Sander, S. P.; Friedl, R. R.; Ravishankara, A. R.; Golden, D. M.; Kolb, C. E.; Kurylo, M. J.; Molina, M. J.; Moortgat, G. K.; Keller-Rudek, H.; Finlayson-Pitts, B. J.; Wine, P. H.; Huie, R. E.; Orkin, V. L. *Chemical Kinetics and Photochemical Data for use in Atmospheric Studies Evaluation Number 15, JPL Publication 06−02*, Jet Propulsion Laboratory: Pasadena, CA, 2006.
(8) Burkholder, J. B.; Mauldin, R. L.; Yokelson, R. J.; Solomon, S.; Ravishankara, A. R. *J. Phys. Chem.* **1993**, *97*, 7597.
(9) Ibuki, T.; Hiraya, A.; Shobatake, K. *J. Chem. Phys.* **1989**, *90*, 6290.
(10) Basco, N.; Hunt, J. E. *Int. J. Chem. Kinet.* **1979**, *11*, 649.
(11) Trolier, M.; Mauldin, R. L.; Ravishankara, A. R. *J. Phys. Chem.* **1990**, *94*, 4896.
(12) Anderson, J. G.; Margitan, J. J.; Stedman, D. H. *Science* **1977**, *198*, 501.
(13) Brune, W. H.; Anderson, J. G.; Chan, K. R. *J. Geophys. Res.* **1989**, *94*, 16649.
(14) Molina, M. J.; Colussi, A. J.; Molina, L. T.; Schindler, R. N.; Tso, T.-L. *Chem. Phys. Lett.* **1990**, *173*, 310.
(15) Rao, Y. V.; Venkateswarlu, P. *J. Mol. Spectrosc.* **1962**, *9*, 173.
(16) Lee, L. C.; Suto, M.; Tang, K. Y. *J. Chem. Phys.* **1986**, *84*, 5277.
(17) Yu, Y. C.; Setser, D. W. *J. Photochem. Photobiol.* **1988**, *42*, 27.
(18) Chichinin, A. I. *J. Chem. Phys.* **2000**, *112*, 3772.
(19) Plenge, J.; Kühl, S.; Vogel, B.; Müller, R.; Stroh, F.; von Hobe, M.; Flesch, R.; Rühl, E. *J. Phys. Chem. A* **2005**, *109*, 6730.
(20) Stimpfle, R. M.; Wilmouth, D. M.; Salawitch, R. J.; Anderson, J. G.; *J. Geophys. Res.* **2004**, *109*, doi:10.1029/2003JD003811.
(21) von Hobe, M.; Grooss, J.-U.; Müller, R.; Hrechanyy, S.; Winkler, U.; Stroh, F. *Atmos. Chem. Phys.* **2005**, *5*, 693.
(22) Avallone, L. M.; Toohey, D. W. *J. Geophys. Res.* **2001**, *106*, 10411.
(23) Cox, R. A.; Hayman, G. D. *Nature* **1988**, *332*, 796.
(24) DeMore, W. B.; Tschuikow-Roux, E. *J. Phys. Chem.* **1990**, *94*, 5856.
(25) Huder, K. J.; DeMore, W. B. *J. Phys. Chem.* **1995**, *99*, 3905.
(26) Burkholder, J. B.; Orlando, J. J.; Howard, C. J. *J. Phys. Chem.* **1990**, *94*, 687.
(27) Atkinson, R.; Baulch, D. L.; Cox, R. A.; Crowley, J. N.; Hampson, R. F.; Hynes, R. G.; Jenkin, M. E.; Rossi, M. J.; Troe, J. *Atmos. Chem. Phys.* **2007**, *7*, 981.
(28) Wilmouth, D. M.; Stimpfle, R. M.; Anderson, J. G.; Elkins, J. W.; Hurst, D. F.; Salawitch, R. J.; Lait, L. R. *J. Geophys. Res.* **2006**, *111*, doi: 10.1029/2005JD006951.
(29) von Hobe, M. *Science* **2007**, *318*, 1878.

JP9053204